Fluid-Thermal Analysis of an Inverter with Air Cooling

Rao V. Arimilli*[1], Ali Hossein Nejad[1], Kivanc Ekici[1]

[1] The University of Tennessee
*414 Dougherty Engineering Building, University of Tennessee, Knoxville, TN 37996-2210, arimilli@utk.edu

Abstract: In this paper, a new and relatively simple air-cooled inverter design is numerically investigated using the COMSOL multiphysics solver. The thermal-fluid analysis is based on a three-dimensional conjugate heat transfer model in which the flow field is assumed to be laminar. A rigorous mesh convergence was performed to ensure that the overall energy balance error is within engineering accuracy while the computational cost is kept within reasonable limits. Three different configurations for the 55-kW inverter (with SiC carbide power electronic devices) design were considered. In all three cases, as a design constraint, the effective cooling surface area was kept constant and the performance of different configurations was investigated. Our initial findings indicate that this new design offers good cooling characteristics. Additionally, the flow rate, pressure drop and blower power requirements are significantly lower relative to turbulent flow configurations. It is shown that COMSOL can model the problem in a reasonably short amount of time.

Keywords: Conjugate Heat Transfer, Laminar flow, Air-Cooled Inverter, SiC, HEV

1. Introduction

The development of power electronics devices with wide-band gap (WGB) materials (e.g., SiC) has made it possible to operate them at higher temperatures than similar Si-based devices [1, 2]. These devices include diodes and IGBTs (Insulated-Gate Bipolar Transistors). Their stability at higher temperatures provides an opportunity to design heat sinks that can be cooled with air instead of liquids [3-6]. Tawfik [5] designed a 55-kW cylindrical shaped air-cooled power inverter configuration for applications related to hybrid electric and plug-in electric transportation vehicles. In that design, the complete inverter is composed of nine power modules. Each module has a mid-plane symmetry and therefore one-half of a module can be used to simulate the heat sink performance. In each half-module, there are four diodes and four IGBTs. The performance parameter of significance to power inverters for automotive use is the power-to-volume ratio. The air-cooled design by Tawfik was shown to meet the performance values for liquid-cooled inverters under turbulent flow conditions. However, other arrangements of modules are possible to achieve comparable performance.

In this study, we considered an alternate in-line arrangement of the modules as opposed to a cylindrical arrangement, using modules of the same size and power dissipation as in Ref. [5]. The half module is utilized in this study and, henceforth, will be referred as the "module" in this paper. As this new inverter configuration is expected to be positioned below or in place of the vehicle radiator, the volume-to-power rating parameter is not likely to be a serious limitation. However, the fin arrangement has to be redesigned for use under laminar flow conditions. This was done, and the results of its performance are presented in this paper.

2. Use of COMSOL Multiphysics

The present analysis is based on conjugate heat transfer with three-dimensional steady-state laminar flow in COMSOL version 4.3b. Figures 1 and 2 show the geometric details of the design configuration and modeled domains. COMSOL version 4.3b was used for all models presented in this paper. The boundary conditions applied can be specified with the aid of Figure 2. They are as follows: 1.) Uniform conditions at the inlet with specified *Redh* and temperature T_i = 300 K; 2.) Zero pressure and zero conductive flux at the exit plane; 3.) No slip and insulated conditions at the two vertical sides; and 4.) Flow and heat transfer symmetry conditions at the top and bottom surfaces.

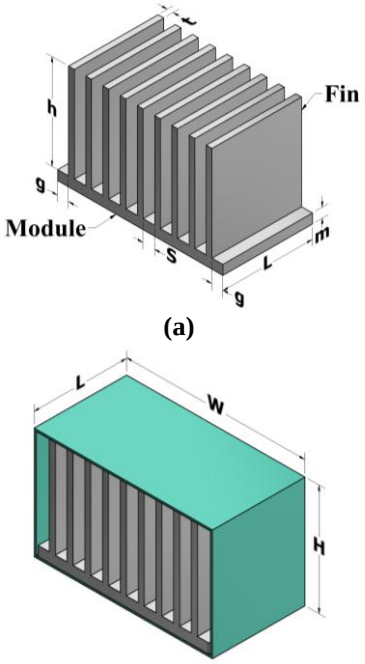

Figure 1. Sketch of the heat sink configuration design.

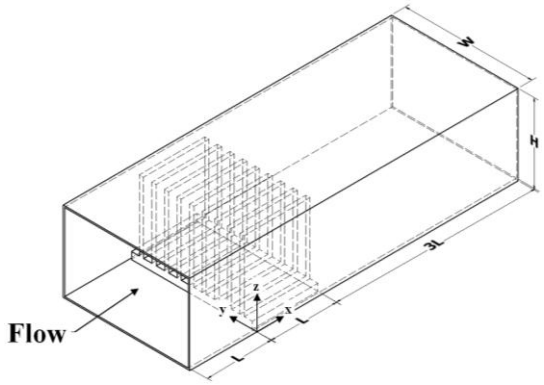

Figure 2. Sketch of the heat sink configuration analyzed in COMSOL showing upstream and downstream flow passage system.

3. Design Methodology for First Configuration

With module geometry already fixed, the fin configurations and sizing and the flow parameters remain to be determined with the objective of maintaining maximum surface temperatures below 200°C while keeping the volume as small as possible. Aluminum is chosen as the material for the module and the fins. The design is to be based on laminar flow operating conditions. The parameters to be determined are *t*, *s*, *h* and N_{fin}. In geometric terms, the fin height has the most influence in limiting the maximum surface temperatures. Preliminary calculations based on single fin performance [7] as well as developing flow through rectangular channels for a range of laminar flow conditions (details not shown in this paper) enabled us to identify h = 50 mm as a viable height for the fins. The fin thickness *t* and spacing *s* were chosen for this first configuration to be 3 and 6 mm, respectively. The configuration was modeled in COMSOL 4.3b and the results show that the temperature objective was achieved for all *ReDh* except 491. To improve temperatures and reduce volume, additional configurations were identified and modeled. The details of this approach are addressed in the body of the paper to avoid repetition.

3.1 Mesh Refinement Study for First Configuration

To ensure that the solution is independent of the mesh used, in addition to the tolerances used to get a converged solution to the problem, the solution must satisfy the First Law of Thermodynamics in a global sense. An obvious measure for a steady state problem is the overall energy balance error (OEBE) defined for the present problem as the ratio of the difference between outlet and inlet energy flow rates to the total power input to the system.

The results should demonstrate that for convergence an overall energy balance error (OEBE) must be satisfied and that it needs to be independent of the mesh used. For a steady-state solution, OEBE should approach zero as the mesh refinement is improved. The results of the mesh refinement study are presented below.
The mesh refinement studies were performed using four different default physics-controlled meshes identified within COMSOL 4.3b as Coarse, Normal, Fine and Finer. They represent a progressively refined sequence of meshes.

Figure 3 (a) shows that OEBE decreases with improved mesh resolution for all inlet Reynolds numbers (*ReDh*) considered. However, OEBE increases with increasing Reynolds number. For all *ReDh* considered, the channel flow Reynolds numbers (*ReDhCh)* for flow within the air

passages between fins based on average velocity at channel inlet and hydraulic diameter is substantially lower. This ensures that the flow everywhere in the channels remains laminar as well. Clearly, at the higher *ReDh* values a much finer mesh is needed to achieve better OEBEs, which is beyond the scope of the resources available for this study.

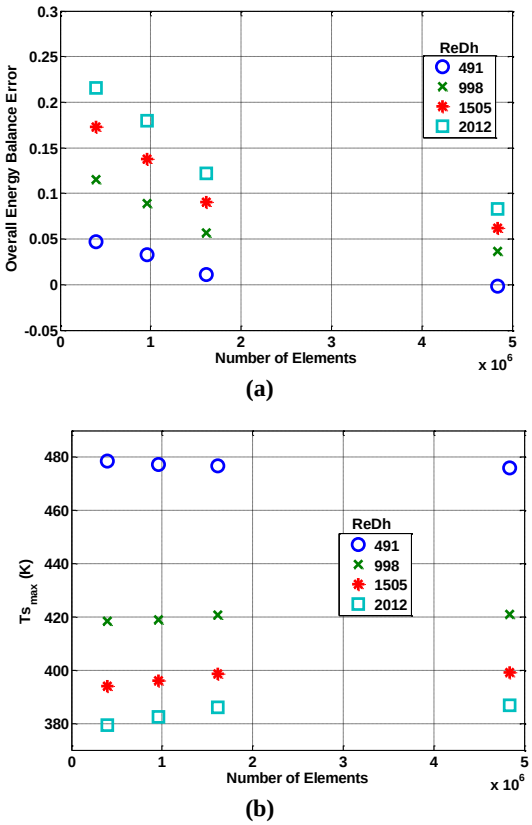

Figure 3. Influence of mesh refinement for various inlet Reynolds numbers *ReDh*. (**a**) Overall energy balance error (OEBE) and (**b**) Maximum surface temperature Ts_{max} for $\boldsymbol{t = 3}$ **mm**, h = 50 mm, s = 6 mm, $\boldsymbol{N_{fin} = 9}$, A_t = 47,636 mm^2.

Figure 3 (b) shows that the variations of maximum temperature, Ts_{max}, were far less sensitive to the mesh refinement. Furthermore, Ts_{max} decreases with increasing *ReDh*. This is in contrast to the much higher sensitivity of the overall energy balance error (OEBE) to mesh refinement. For the finest two meshes, the variation in Ts_{max} is less than 1 K. Further, for this first configuration considered, the lowest Reynolds number case has the most accurate solution and has the highest Ts_{max} of about 480 K (207°C). For the Tawfik [5] design, with its internal configuration of IGBTs and diodes within the module, the maximum device temperature (IGBT or Diode) is about 5 K above the maximum surface temperature of the module. With that knowledge, for the present configuration we can be sure that the device temperatures will be higher by about 5°C, resulting in a maximum device temperature of 212°C. Such maximum temperatures are within the acceptable operating range of SiC devices used for power electronics applications. The values of Ts_{max} from Figure 3b are tabulated in Table 1.

Table 1. Ts_{max}(K) variation as a function of *ReDh* and Mesh refinement for $\boldsymbol{t = 3}$ **mm**, h = 50 mm, s = 6 mm, $\boldsymbol{N_{fin} = 9}$, $\boldsymbol{A_t = 47{,}636}$ **mm**^{2}.

ReDh	491	998	1505	2012
Mesh	Ts_{Max} (K)			
Coarse	478.54	418.5	394.15	379.31
Normal	477.31	418.93	396.12	382.35
Fine	476.72	420.66	398.65	386
Finer	475.92	420.91	399.23	386.72

3.2 Additional Configurations

For a good inverter design, it is desirable to keep the maximum device temperature below 200°C for all *ReDh*, and reduce the overall dimension of the inverter to make it more compact and lighter. This can be achieved by some combination of increasing the number of fins N_{fin}, reducing fin thickness t, and decreasing height of fins h to values below 50 mm. Additionally, reduction of fin thickness may reduce the overall weight of the inverter depending on the number of fins chosen. However, as the inverter will be directly exposed to highway air, it is likely to encounter particulate-laden flow during some periods of its operation. Therefore, we limit ourselves to minimum fin thickness of 2 mm for its robustness relative to smaller thicknesses.

Since the module dimensions are fixed, the reduction of fin height is the primary design parameter to reduce the overall size of the inverter. The results shown in Figure 3 for the first configuration considered (t = 3 mm, N_{fin} = 9, and h = 50 mm) produced acceptable maximum surface temperatures. The area exposed to air can be increased, while keeping h unchanged, by

reducing t and correspondingly increasing N_{fin}. It would be instructive to explore the influence of increased surface area on the extent to which Ts_{max} can be reduced. We begin by first reducing the fin thickness to 2 mm and increasing N_{fin} to 11. This choice of N_{fin} ensures that the gap g is less than $s/2$. This case was modeled in COMSOL and the results for Ts_{max} are given in Table 2.

Table 2. Ts_{max}(K) variation as a function of *ReDh* and Mesh refinement. For $\boldsymbol{t = 2}$ **mm**, h = 50 mm, s = 6 mm, $\boldsymbol{N_{fin} = 11}$, $\boldsymbol{A_t = 56{,}738\ mm^2}$.

ReDh	491	998	1505	2012
Mesh	Ts_{Max} (K)			
Coarse	466.43	409.44	386.98	373.43
Normal	464.67	409.48	388.76	376.6
Fine	465.08	411.05	389.97	377.9
Finer	464.28	411.48	390.7	*

*The solution for this configuration did not converge.

As shown in Table 2, the values of Ts_{max} are lower by about 9°C compared to the corresponding values in Table 1. The effect of change in t and N_{fin} result in an increase in area exposed to heat transfer (A_t) by 19% and reduction of Ts_{max} by about 9°C. As t cannot be reduced any further (basis for this design) to maintain the desired temperatures, the area exposed to heat transfer has to be maintained as close to A_t = 56,738 mm^2 as possible. This can be achieved by reducing h and s and increasing N_{fin}. With this in mind, the following configurations shown in Table 3 are identified for further performance evaluation.

Table 3. Configurations considered for performance evaluations

Case	t (mm)	h (mm)	s (mm)	N_{fin}	A_t (mm^2)
A	2	50	6	11	56738
B	2	42	4.5	13	56160
C	2	33	3	17	57251

4. Performance of Additional Configurations

The performance of each of the three configurations shown in Table 3 is evaluated at the four laminar flow conditions, namely *ReDh* of 491, 998, 1505 and 2012. Clearly, as *ReDh* increases inlet velocity U increases. For case A, a detailed mesh sensitivity analysis was performed and the results for OEBE, Ts_{max} and the overall pressure drop, DP, are shown in Figure 4.

Figure 4 (a) shows OEBE decreasing with improved mesh refinement for all inlet Reynolds numbers *ReDh* considered. It should be pointed out that these errors are lower than the results shown in Figure 3 (a). However, in both cases, OEBE increases with increasing *ReDh*. At the higher *ReDh*, a much finer mesh is needed to achieve better OEBE, which is beyond the scope of the computational and time resources available for this study.

Figure 4 (b) shows that the variations of maximum temperature, Ts_{max}, were less sensitive to the mesh refinement, much like the results in Figure 3 (b). If only the maximum temperatures are of interest, a coarse mesh solution may be adequate.

However, Figure 4 (c) shows the pressure drop to be more sensitive to mesh refinement in a manner similar to overall energy balance error. The pressure drops are quite small, less than 5 Pa. Therefore, there is no need for additional mesh refinements. The error of pressure drop results are shown Table 4. It should be noted that the pressure drops obtained with the Normal mesh are always higher than those of the Finer mesh. In other words, the results from the Normal mesh are over estimating the pressure drop.

Table 4. The error in pressure drop of Normal mesh relative to Fine and Finer meshes, for t = 2 mm, h = 50 mm, s = 6 mm, N_{fin} = 11, A_t = 56738 mm^2.

ReDh	491	998	1505	2012
%Error relative to **Fine** mesh	2.79	2.3	3.03	3.57
%Error relative to **Finer** mesh	4.45	5.66	7.35	*

*The solution to this configuration did not converge.

In light of the computational resource limitations mentioned before, the alternate configurations to be discussed will be solved using the Normal mesh.

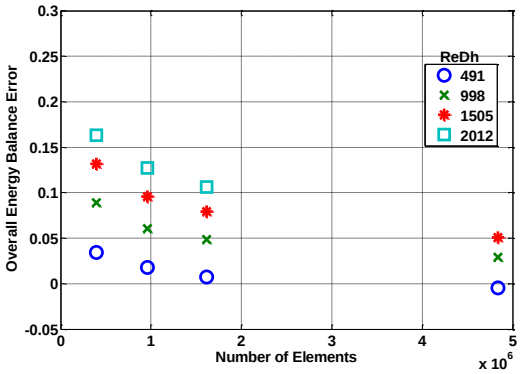

(a)

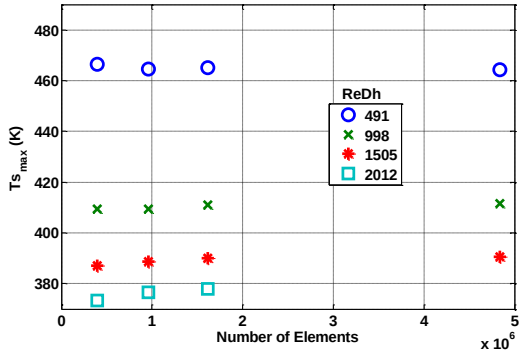

(b)

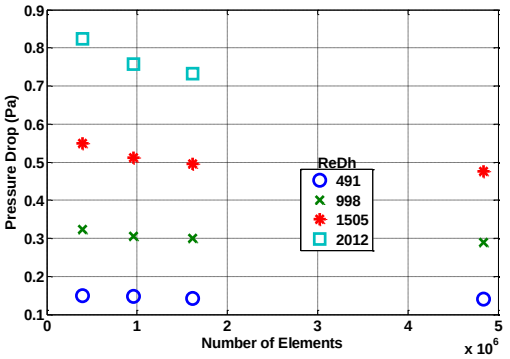

(c)

Figure 4. Influence of mesh refinement for various *ReDh*. (**a**) Overall energy balance error (OEBE), (**b**) Maximum temperature Ts_{max} and (**c**) Overall pressure drop, for ***t* = 2 mm**, h = 50 mm, s = 6 mm, $\boldsymbol{N_{fin}}$ **= 11**, A_t = 56,738 mm^2. For Finer mesh with *ReDh* = 2012, the solution did not converge.

4.1 Results for Configurations A, B and C

As the Normal mesh results for all these cases are being presented here, these results represent Ts_{max} values that are slightly lower and *DP* values that are overestimated compared to the Finer mesh solution.

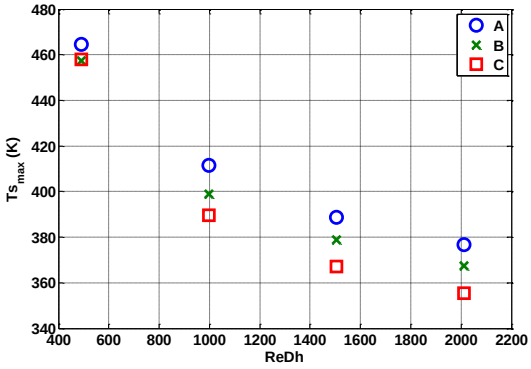

(a)

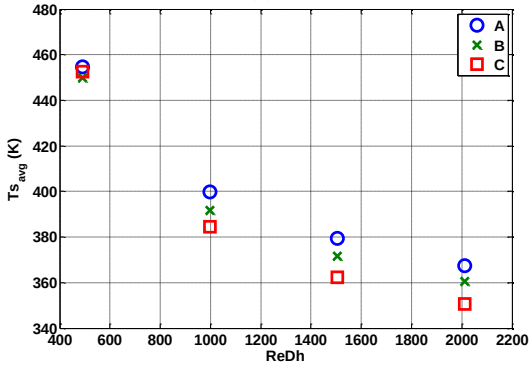

(b)

Figure 5, (a) Maximum surface temperature Ts_{max} and (**b**) Average surface temperature Ts_{avg}, for configurations A,B and C.

Figure 5a and 5b show that the Ts_{max} and Ts_{ave} decrease rapidly with increasing *ReDh*. As can be seen, Case A has the highest temperatures, and Case C has the lowest temperatures. There is very little difference between the maximum and the average temperatures of the surfaces, the difference being less than 10°C.

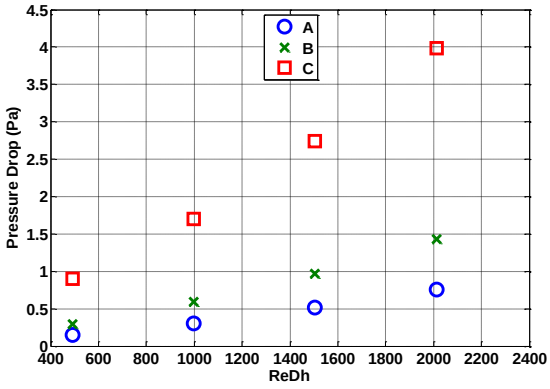

Figure 6, Pressure drop for configurations A,B and C.

Figure 6 shows the overall pressure drop increases as the height of the fins is decreased and the number fins is increased (Case A to Case C).

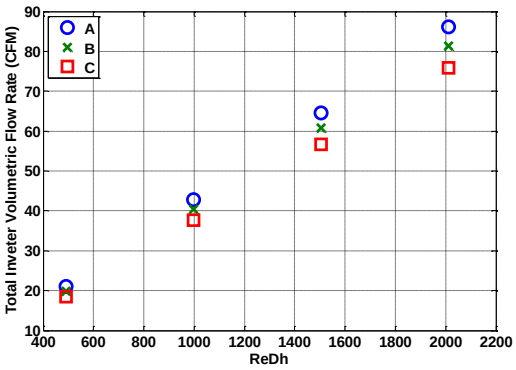

Figure 7. Total inverter volumetric flow rate *Q* for configurations A,B and C.

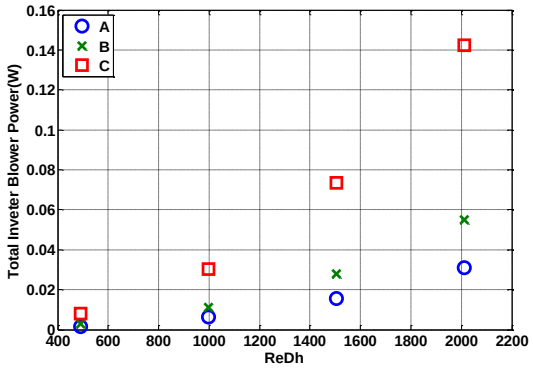

Figure 8. Total inverter blower power input for configurations A, B and C.

Figure 7 shows that the total volumetric flow rate at the inlet for the entire inverter, composed of 18 half modules, increases linearly as the Reynolds number is increased. The total inverter blower power input (= *Q.DP*) vs *ReDh* is shown in Figure 8. These blower power requirements are far lower than those reported in Tawfik's work [5], which has a very complex configuration with turbulent flow and other additional requirements, which are external to the module itself.

4.2 Evolution of Temperature and Velocity Fields for Case A

The solution flow fields for Case A (t = 2 mm, s = 6 mm, h = 50 mm) for *ReDh* of 491 are presented in Figures 10 through 13 and discussed next.

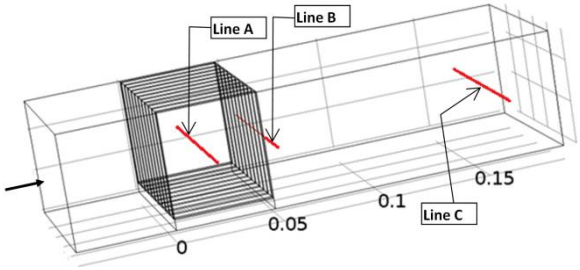

Figure 9. The location of cut lines A, B and C for presenting velocity and temperature distributions. These lines span the width of the duct.

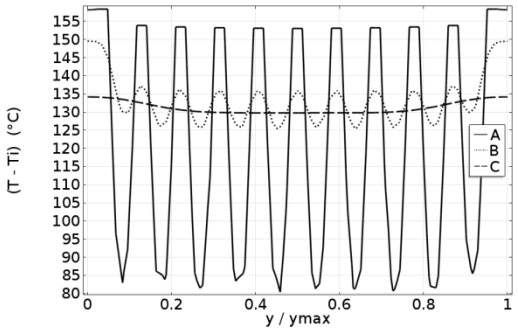

(a)

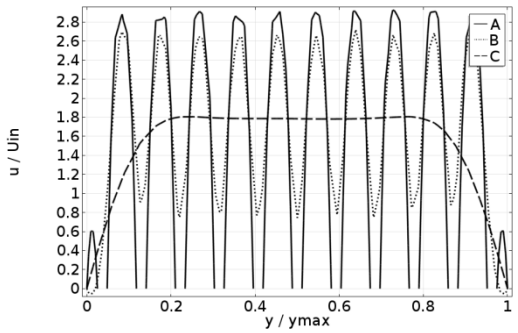

(b)

Figure 10. Line plot of (a) temperature above the inlet temperature and (b) dimensionless velocity at *ReDh* = 491 for Case A at cut lines A, B and C shown in Figure 9.

In Figure 9, the cut line A cuts through the fins and the air, line B is just downstream of the fins where the medium is all air, and line C is far downstream where the fluid velocity and temperature should show the wake effect of the fins being redistributed and having a distribution representative of an incipient fully-developed flow.

In Figure 10(a), the distribution of temperature above the inlet temperature is shown. At cut line A, the temperature plateau is the temperature of the fin and the valley represents the temperature distributions of the fluid between fins. The temperature range of the fluid is quite large. However, at line B the fluid temperatures redistribute rapidly to a higher average temperature level, with some oscillations of amplitude of 5°C everywhere except at the two sides near the walls, where the T-T_i is about 15°C higher. The primary reason for this is that the channel width g is narrower than $s/2$ resulting in a lower average velocity in the gap [see Figure 7(b)]. This results in a higher temperature for this portion of the flow. When the flow reaches close to the exit (at line C), the temperatures redistribute more uniformly and the resulting distribution does not have spacial oscillations. However, the temperatures near the walls continue to be higher compared to those near the center of the channel.

In Figure 10(b), the dimensionless velocity distribution is shown. At line A, the centerline velocity between the fins peaks at a velocity 2.8 times that of the inlet velocity. However, at line B the fluid velocity decelerates slightly to 2.6 times that of the inlet velocity. At the two sides, the velocity is quite low and the peak is 60 percent of the inlet velocity. When the flow reaches close to the exit (at line C), the velocities redistribute having a form that is representative of an incipient fully-developed flow.

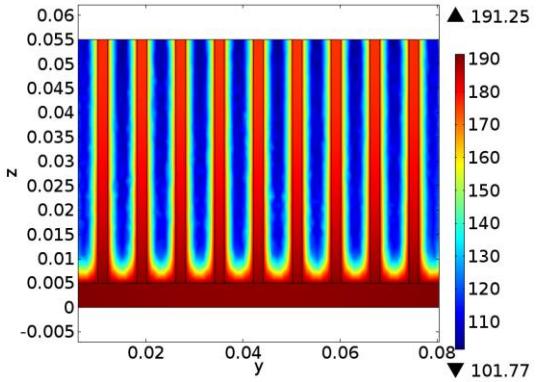

Figure 11. Module, fin and fluid temperature (in °C) distribution in Y-Z plane through Line A in Figure 9 for *ReDh* = 491 for Case A

Figure 11 shows the temperature distribution in a plane normal to the flow direction and passing through the line B. The temperature of the module is quite uniform and the fin tip temperature drops by about 10°C from the temperature of the module. Temperature drop of the fins from root to tip is quite small and this generally higher temperature aids the heat transfer to the fluid.

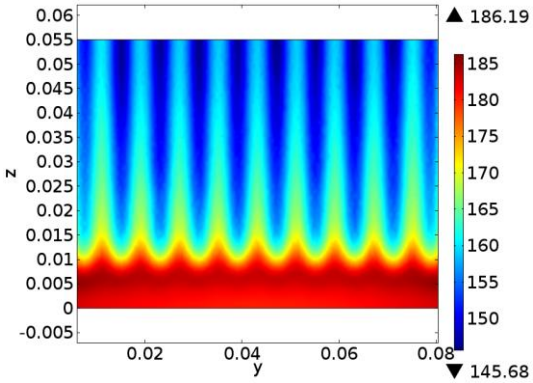

Figure 12. Fluid temperature (in °C) distribution in Y-Z plane through Line B in Figure 9 for *ReDh* = 491 for Case A

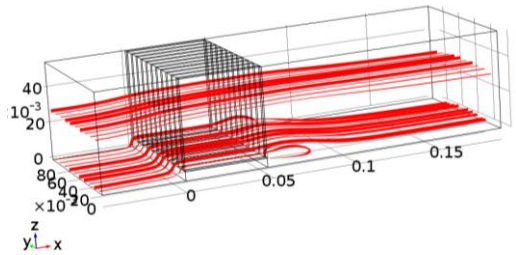

Figure 13. Select streamlines Case A for Re = 491 (t = 2 mm, s = 6 mm, h = 50 mm).

Shown in Figure 12 is the temperature distribution through line B in the y-z plane. Energy redistribution relative to that in Figure 11 can be seen by noticing minimum temperature increase by about 45°C and a decrease of maximum temperature by about 5°C.

Finally, Figure 13 shows two sets of streamlines. Those starting at the mid-height of the duct inlet show a slight upward deflection as they pass through the fins. The streamlines that originate very close to the bottom surface show the upward deflection due to the presence of the module, and the flow behind the module shows recirculation.

5. Conclusions

The objective of this study was to design a laminar flow air-cooled heat sink for a 55-kW inverter, typically used in hybrid electric vehicles, that meets the maximum operating temperature limits of the SiC-based power electronic devices within the inverter. This objective was successfully achieved for three different configurations. A rigorous mesh convergence analysis showed that the solution satisfied the overall energy balance within engineering accuracy while the computational cost is kept within reasonable limits. From the results for the range of parameters considered, the following conclusions are drawn: (a) All three configurations satisfy the device maximum operational temperatures; (b) The pressure drop, volumetric flow rate and blower power requirements in every case are significantly lower relative to similar turbulent fluid flow conditions; (c) The maximum temperatures decrease with increasing Reynolds numbers; and (d) The volume of inverter decreases with decreasing height of the fins. The selection of a particular design depends on the under-the-hood space available for a given application. The designs also permit more than one arrangement of the modules to form a complete inverter.

6. References

1. M. Chinthavali, L. M. Tolbert, H. Zhang, J. H. Han, F. Barlow, and B. Ozpineci, "High power SiC modules for HEVs and PHEVs," in IEEE Power Electronics Conference (IPEC), 2010 International, pp. 1842–1848, 2010.

2. D. C. Katsis and Y. Zheng, "Development of an extreme temperature range silicon carbide power module for aerospace applications," in IEEE Power Electronics Specialists Conference, 2008, pp. 290–294.

3. D. Bortis, B. Wrzecionko, and J. W. Kolar, "A 120C Ambient Temperature Forced Air-Cooled Normally-off SiC JFET Automotive Inverter System," IEEE Applied Power Electronics Conference and Exposition (APEC), 6-11 March 2011, pp. 1282 – 1289.

4. M. Chinthavali, P. Otaduy, B. Ozpineci, "Comparison of Si and SiC Inverters for IPM Traction Drive," IEEE Energy Conversion Congress and Exposition, September, 2010, pp. 3360-3365.

5. Jonathan A. Tawfik, Thermal Feasibility and Performance Characteristics of an Air-Cooled Axial Flow Cylindrical Power Inverter by Finite Element Analysis, M.S. Thesis, The University of Tennessee, Knoxville, May 2011.

6. Chinthavali, Madhu , J. A. Tawfik, and R. V. Arimilli, Design and Analysis of a 55-kW Air-Cooled Automotive Traction Drive Inverter, Energy Conversion Congress and Exposition (ECCE), 2011 IEEE, PID1930289.pdf.

7. F. P. Incropera and D.P. DeWitt, *Fundamental of Heat and Mass Transfer*, 5th edition, John Wiley & Sons, 2002.

7. Nomenclature

A_t	Total solid surface area exposed to fluid (mm^2)
Dh_{in}	Hydraulic diameter at the inlet (mm) = $2(m+h)W/(m+h+W)$
Dh_{ch}	Hydraulic diameter of channel between fins (mm) = $2\ s\ h/(s+h)$
DP	Overall pressure drop (Pa) = $P_{avg,inlet} - P_{outlet}$
Eg	Energy generation in half module (W)
g	Gap as shown in Figure 1 (mm)
h	Height of fin (mm)
m	Half thickness of module (mm)
N_{fin}	Number of fins
P	Pressure (Pa)
$P_{avg,inlet}$	Average pressure at inlet surface (Pa)
P_{outlet}	Average pressure at outlet surface (Pa)
Q	Inlet volumetric flow rate (CFM)
$ReDh$	Reynolds number at inlet = $\rho\ U_{in}\ Dh_{in}/\mu$
$ReDhCh$	Reynolds number at inlet = $\rho\ U_{ch}\ Dh_{ch}/\mu$
s	Spacing between fins (mm)
t	Thickness of fin (mm)
T	Temperature (K)
T_i	Inlet air temperature (K)
T_s	Surface temperature of solid domain (K)
Ts_{max}	Maximum surface temperature of solid domain (K)
Ts_{avg}	Average surface temperature of solid domain (K)
T_{bo}	Outlet fluid bulk temperature (K)
u	Local x-velocity (m/s)
U_{ch}	Average velocity at inlet to channel (m/s)
U_{in}	Inlet velocity (m/s)
W	Width of the module (mm)
Greek Letters	
ρ	Density (Kg/m^3)
μ	Dynamic viscosity (N.s/m^2)